2015 International Symposium on Nonlinear Theory and its Applications
NOLTA2015, Kowloon, Hong Kong, China, December 1-4, 2015

Bifurcation Analysis of Subsynchronous Oscillations in DFIG Wind Farms

Gustavo Revel, Andres E. Leon, Diego M. Alonso and Jorge L. Moiola

Instituto de Investigaciones en Ing. Eléctrica (IIIE) Alfredo Desages (UNS-CONICET)
Depto. de Ing. Eléctrica y de Computadoras, Universidad Nacional del Sur
Av. Alem 1253, (8000) Bahía Blanca, Argentina
Email: grevel@uns.edu.ar

Abstract—This work studies the dynamics associated to subsynchronous interactions between wind farms and series compensated ac transmission systems. This interaction originates large amplitude oscillations, which drives the system to the instability and may also produce a severe damage to the equipment. The analysis is based on bifurcation theory and it is carried out using continuation tools, in order to determine the role that typical parameters (e.g., the compensation level and the wind speed) have on the phenomenon. The bifurcation study reveals that the underlying mechanism associated with the appearance of subsynchronous oscillations can be explained by means of Hopf bifurcations of the equilibrium point and their corresponding limit cycles.

1. Introduction

The addition of large scale wind farms (WFs) to existing power systems introduces new challenges to the design and operation of the system. For example, when a WF consisting of doubly-fed induction generators (DFIGs, or type-3 machines), becomes radially connected to long series compensated transmission lines[1], dangerous interactions between the turbines and the electric grid can arise. This phenomenon is known as subsynchronous interaction (SSI), and a renown incident occurred in Texas in 2009, when after a contingency two WFs became radially connected to a series compensated line. The new system configuration (post-fault) produced a SSI event a few seconds after the fault was cleared, and large amplitude subsynchronous oscillations developed on the system, causing severe damages not only to the capacitor bank but also to the wind turbines [1]. This incident captured the attention of system operators as well as power system researchers, triggering a series of studies dedicated to the description of the problem and to the analysis of mitigation proposals [2, 3].

Nonlinear analysis techniques such as bifurcation theory, has been successfully used in the last few years to study the dynamical behavior of power systems, including the integration of renewable sources [4, 5]. Moreover, the bifurcation theory was used to analyze subsynchronous torsional interactions in conventional synchronous generators [6]. In this work, bifurcation theory is used to describe the dynamics emerging at subsynchronous interactions between DFIG wind turbines and series compensated lines. The model used consists of a WF represented by an equivalent DFIG wind turbine (aggregated model), connected to an equivalent network via a series compensated transmission line. Two representative bifurcation parameters are used to characterize the SSI phenomenon: i) the compensation level, defined as the ratio between the capacitive and inductive reactances of the transmission line (i.e. $\mu = X_C/X_L$); and ii) the wind speed (v_{wind}). One- and two-parameter bifurcation diagrams are obtained using the numerical continuation software Cl_MatCont [7]. The analysis provides a clear information about the influence of the bifurcation parameters on the SSI phenomenon, revealing the mechanisms responsible for the lost of the local stability of the operating point (equilibrium), as well as the amplitude and stability of the emerging periodic solutions. Since the control scheme of the WF includes saturation limits, other singularities such as non-smooth grazing bifurcations of periodic orbits are also detected. Finally, the results are resumed in a two-parameter bifurcation diagram where a generalized Hopf bifurcation acts as the organizing center of the dynamics.

The paper is organized as follows. The power system model used as case study is described in Sec. 2. The bifurcation analysis of the SSI phenomenon is performed in Sec. 3, and the concluding remarks are given in Sec. 4.

2. Power system model for SSI studies

A schematic representation of the power system used in this paper is shown in Fig. 1. The model consist of a 500 MVA aggregated DFIG wind farm, radially connected to an equivalent network (7000 MVA, 50 Hz) via a series capacitive compensated transmission line of 354 km. The DFIG uses back-to-back power converters (the rotor-side converter (RSC) and the grid-side converter (GSC) in Fig. 1) to control the generated active and reactive powers. The implemented vector control scheme is shown in Fig. 2 (see details in [8]).

The RSC controls the total active power (P_{total}) and the reactive power (Q_{total}) injected to the grid. The active power reference (P^{ref}_{total}) is computed by means of the ac-

[1]The radial connection between the wind farm and the compensated line may not occur in normal operation, but instead it may be due to a system re-configuration after a fault.

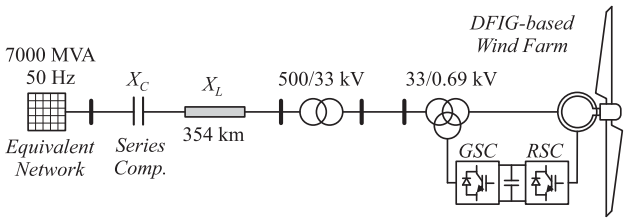

Figure 1: Schematic representation of the power system considered for the study of SSI.

tive current (i_A^{ref}) in order to extract the maximum power from the wind (using a maximum power point tracking (MPPT) algorithm). The reactive power reference (Q_{total}^{ref}) is obtained through the reactive current reference (i_R^{ref}) in order to regulate the terminal voltage. The magnitude of reference currents and voltages are limited to protect the equipment. For example, the active and reactive reference currents in the RSC are limited so that the maximum apparent current [i_S^{max} in Fig. 2(a)] is not exceeded. The RSC prioritizes the reactive power injection, to support the terminal voltage in case of a fault (satisfying the grid code regulations). Then, the maximum active current reference is calculated as $i_A^{max} = \sqrt{(i_S^{max})^2 - (i_R^{ref})^2}$, and $i_A^{ref} \leq i_A^{max}$. Notice that, when $i_R^{ref} = i_S^{max}$ then $i_A^{max} = i_A^{ref} = 0$. Similar limitation schemes (with $Q-axis$ priority) are adopted for the remaining signals of the RSC [see Fig. 2(a)]. The rotor current references i_D^{ref} and i_Q^{ref}, are calculated by a couple of proportional-integral (PI) controllers in order to achieve the desired active and reactive power, respectively. These references are limited by the maximum apparent current of the rotor (i_{rot}^{max}), prioritizing the reactive component i_Q^{ref}. It will be seen in Sec. 3, that this limit has an important role in the dynamics. Finally, the voltages applied to the rotor (v_D and v_Q) are calculated by means of inner control loops also using a couple of PI controllers (plus feedforward compensation terms v_D^{comp} and v_Q^{comp}). These control actions are limited by the maximum rotor voltage, v_{rot}^{max}.

The GSC uses the active current (i_{gd}) to maintain the voltage on the dc-link at its reference value (v_{cd}^{ref}), while its reactive current (i_{gq}) is regulated to zero[2] ($Q_{gsc}^{ref} = 0$). The control strategy is similar to the one explained for the RSC, nevertheless the GSC prioritizes the active current component, since it is used to maintain the voltage of the dc-link.

3. Dynamical analysis of SSI

The complete power system model has 33 state variables, and since the signals of the DFIG vector control have saturation limits, the system can be classified as piecewise smooth continuous (PWSC), with multiple switching boundaries given by the maximum modules of the control

[2]The reactive current of the GSC may be used by a supplementary controller in order to damp oscillations.

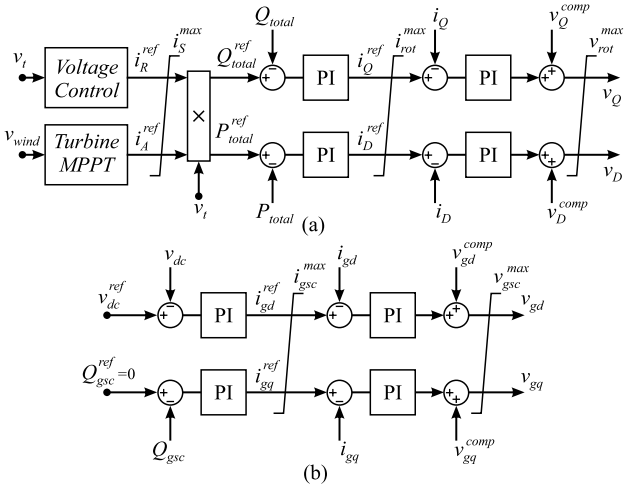

Figure 2: DFIG vector control. (a) RSC, the limits have reactive power priority. (b) GSC, with active power priority.

signal, i.e., i_S^{max}, i_{rot}^{max} and v_{rot}^{max} for the RSC, and i_{gsc}^{max} and v_{gsc}^{max} for the GSC. This means that the vector field is continuous across the switching boundaries, but the Jacobian is discontinuous. It will be seen later that the limitation of the control signals plays an important role in the dynamics, since they induce grazing bifurcations of periodic orbits [9, 10]. The numerical continuations are performed using Cl_MatCont [7]. This package provides great flexibility to perform continuations in high dimensional systems. Although it is designed to work with ODE systems, in this case, the continuation algorithm proved to be robust enough to follow the periodic orbits after the grazing bifurcations. Notice that the discontinuous bifurcations are not detected by this package.

In order to illustrate the mechanism behind the SSI phenomenon, let us start by considering the locus of the eigenvalues in response to the variation of the compensation level μ. Figure 3 shows the loci of the most relevant eigenvalues (only the positive imaginary part is shown), when the compensation level μ goes form 1% to 100%, for two wind speeds: 6.5 m/s (blue dots) and 8.0 m/s (green dots). In both cases, the squares indicate the position of the eigenvalues when $\mu = 1\%$, the empty circles correspond to $\mu = 50\%$ and the triangles to $\mu = 100\%$. When the compensation is very low ($\mu = 1\%$), the subsynchronous mode has an acceptable damping for both wind conditions. When μ is increased, this mode moves towards the imaginary axis, decreasing both frequency and damping. On the other hand, the supersynchronous mode moves towards the left, increasing the frequency, with a small reduction on the damping factor (less considerable than the one suffered by the subsynchronous mode). In both cases, the equilibrium point becomes unstable when the subsynchronous mode crosses the imaginary axis, undergoing a Hopf bifurcation.

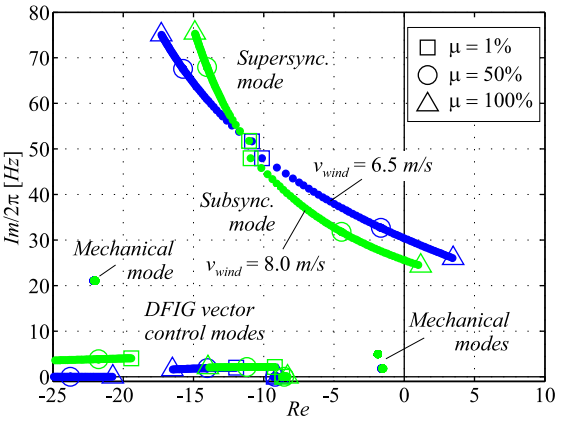

Figure 3: Loci of the most relevant eigenvalues varying μ for v_{wind} = 6.5 m/s (blue) and v_{wind} = 8.0 m/s (green).

3.1. One-parameter bifurcation analysis of SSI

In order to analyze the Hopf bifurcations associated to the subsynchronous mode, one-parameter bifurcation diagrams were obtained varying μ, as shown in Fig. 4. The stable equilibrium points are depicted with solid blue lines, the unstable equilibria with dashed red lines and the Hopf bifurcations ($H^{\pm}$, where the superscript indicates the sign of the Lyapunov index) are indicated with blue dots. Stable limit cycles are represented with black circles, and the unstable cycles with empty circles. The red dots are grazing bifurcations of the limit cycle, and the solid (dashed) gray line indicates what would be the amplitude of the stable (unstable) limit cycle if the system does not have limits on the vector control signals.

Let us begin the description by considering the case with v_{wind} = 6.5 m/s of Fig. 4(a). Here, the Hopf bifurcation is supercritical (H^-), and a stable limit cycle emerges towards the right. The amplitude of this cycle rapidly increases until a grazing bifurcation occurs, when the maximum apparent rotor current (i_{rot}^{max}) is reached [red dot in Fig. 4(a)]. Then, for increasing values of μ, the cycle remains stable but with an almost constant amplitude. The effect of the grazing bifurcation becomes notorious when the actual cycle is compared with the non-limited cycle (gray line).

The second case for v_{wind} = 8.0 m/s is shown in Fig. 4(b). Now, the Hopf bifurcation is subcritical (H^+) and an unstable cycle emerges towards the left. The amplitude grows until the maximum rotor current limit is reached. In this case the grazing bifurcation is a non-smooth saddle-node of limit cycles. This bifurcation annihilates the unstable cycle that in the non-limited case would evolve to the left (gray dashed line) and introduces a stable one to the right (with a bistability region near H^+).

Notice that in both diagrams the cycles are the same as their non-limited versions, until the grazing occurs. Moreover, there is a difference between the grazing bifurcation of Figs. 4(a) and 4(b): in the first one the limit cycle *persists* and conserve its stability after the singularity, while in the

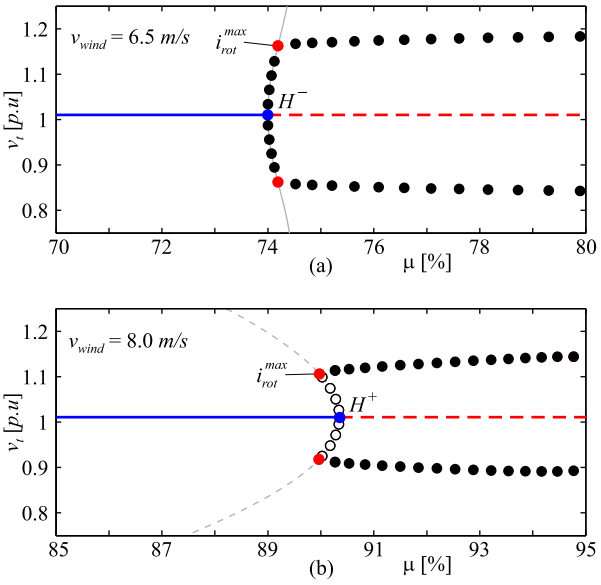

Figure 4: One-parameter bifurcation diagrams varying μ. (a) v_{wind} = 6.5 m/s. (b) v_{wind} = 8.0 m/s.

latter case the grazing induces a *non-smooth saddle-node* bifurcation.

Finally, it is worth to mention that in the considered application, non-smooth bifurcations appear only at limit cycles. They do not arise at the equilibrium points (known as Boundary Equilibrium Bifurcation (BEB) [10]), since when the WF operates at nominal conditions, the reference signals do not reach the limits (although they might be transiently limited due to a perturbation).

3.2. Two-parameter bifurcation analysis of SSI

The changes in the dynamics observed between the two bifurcation diagrams of Fig. 4 can be related to a generalized Hopf bifurcation and can be explained by performing a two-parameter bifurcation analysis varying μ and v_{wind}, simultaneously. The resulting diagram is shown in Fig. 5, where the blue curve corresponds to a Hopf bifurcation (solid when it is supercritical and dashed when it is subcritical), and the red one denotes grazing bifurcations of limit cycles (solid when it is a non-smooth saddle-node and dashed-dotted when the cycle persists with the same stability). The dotted lines indicate the slices shown in Fig. 4.

By simple inspection of the Hopf curve, it is clear that for a fixed value of μ the equilibrium point becomes unstable when the wind speed decreases. Moreover, the change from H^- to H^+ occurs when the Lyapunov index of the Hopf bifurcation vanishes. This codimension-two bifurcation is known as generalized Hopf (GH) and it is indicated by the black dot in Fig. 5. The rapid increment on the amplitude of the stable limit cycle shown in Fig. 4(a) is associated to the proximity of the point GH. Moreover, the amplitude of the oscillation remains almost constant after crossing the grazing curve (dashed-dotted red). The graz-

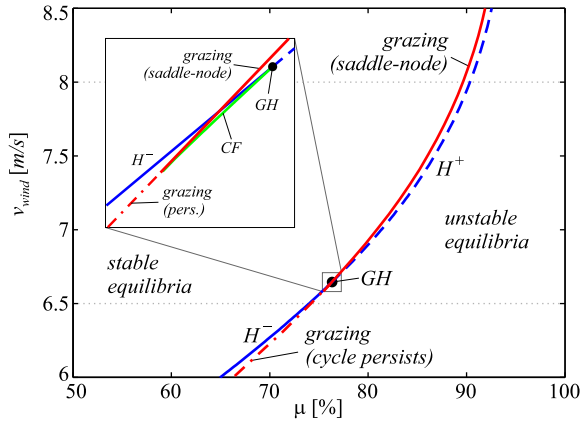

Figure 5: Two-parameter bifurcation diagram varying μ and v_{wind}, simultaneously.

ing (saddle-node) curve in Fig. 5 remains very close to the Hopf curve. This is a positive fact for the wind farm stability since the unstable limit cycle emerging from H^+ only exist in a small region close to the Hopf curve. Finally, as shown in the blow-up of Fig. 5, the smooth saddle-node of periodic cycles (solid green curve, CF) that emerges at GH, interacts with the grazing bifurcation curve in a codimension-two bifurcation of limit cycles. This singularity changes the type of grazing bifurcation from the one in which the limit cycle persists to the one that generates a non-smooth saddle-node (a similar structure is analyzed in [11]). This interaction will be studied in the future.

4. Conclusions

This paper shows that the dynamical phenomena involved with SSI are organized by a generalized Hopf bifurcation and grazing bifurcations of limit cycles. The generalized Hopf denotes that the stability of the limit cycle emerging form the Hopf bifurcation can change depending on the parameters. Moreover, when the Hopf bifurcation is supercritical, the amplitude of the stable limit cycle rapidly grows until it suffers a grazing bifurcation, then it remains practically constant. On the other hand, when Hopf bifurcation is subcritical, the emerging unstable limit cycle vanishes due to a non-smooth saddle-node generated by a grazing bifurcation. This prevents the unstable cycle from affecting the stable operating region, and the main effects related to the SSI appears on the right of the bifurcation curves denoted in Fig. 5. Moreover, the controller limits restrict the amplitude of the oscillation.

Acknowledgments

This work was supported by UNS (PGI 24/K064), ANPCyT (PICT 2014-2161) and CONICET (PIP 112-2012 01-00144).

References

[1] ERCOT, "CREZ reactive power compensation study," ABB, Raleigh, USA, Tech. Rep. E3800-PR-02, Dec. 2010.

[2] B. Badrzadeh, M. Sahni, Y. Zhou, D. Muthumuni, and A. Gole, "General methodology for analysis of sub-synchronous interaction in wind power plants," *IEEE Trans. Power Syst.*, vol. 28, no. 2, pp. 1858–1869, May 2013.

[3] A. E. Leon and J. A. Solsona, "Sub-synchronous interaction damping control for DFIG wind turbines," *IEEE Trans. Power Syst.*, vol. 30, no. 1, pp. 419–428, Jan. 2015.

[4] X. Xiong, C. Tse, and X. Ruan, "Bifurcation analysis of standalone photovoltaic-battery hybrid power system," *IEEE Trans. Circuits Syst. I, Fundam. Theory Appl*, vol. 60, no. 5, pp. 1354–1365, May 2013.

[5] G. Revel, A. E. Leon, D. M. Alonso, and J. L. Moiola, "Dynamics and stability analysis of a power system with a PMSG-based wind farm performing ancillary services," *IEEE Trans. Circuits Syst. I, Fundam. Theory Appl*, vol. 61, no. 7, pp. 2182–2193, July 2014.

[6] A. H. Nayfeh, A. Harb, C.-M. Chin, A. M. Hamdan, and L. Mili, "A bifurcation analysis of sub-synchronous oscillations in power systems," *Electr. Power Syst. Res.*, vol. 47, no. 1, pp. 21–28, 1998.

[7] A. Dhooge, W. Govaerts, Y. A. Kuznetsov, H. G. E. Meijer, and B. Sautois, "New features of the software MatCont for bifurcation analysis of dynamical systems," *Math. Comput. Model. Dyn. Syst.*, vol. 14, no. 2, pp. 147–175, 2008.

[8] A. Tapia, G. Tapia, J. X. Ostolaza, and J. R. Sáenz, "Modeling and control of a wind turbine driven doubly fed induction generator," *IEEE Trans. Energy Convers.*, vol. 8, no. 2, pp. 194–204, Jun. 2003.

[9] I. A. Hiskens and P. B. Reddy, "Switching-induced stable limit cycles," *Nonlinear Dyn*, vol. 50, pp. 575–585, 2007.

[10] M. di Bernardo, C. Budd, A. Champneys, and P. Kowalczyk, *Piecewise-smooth Dynamical Systems. Theory and Applications*. London: Springer-Verlag, 2008.

[11] V. Avrutin, E. Fossas, A. Granados, and M. Schanz, "Virtual orbits and two-parameter bifurcation analysis in a ZAD-controlled buck converter," *Nonlinear Dyn*, vol. 63, no. 1–2, pp. 19–33, Jan. 2011.